A concentration-dependent differential AKT phosphorylation regulation between the breast normal and tumor cells induced by the flavonoids in Macrothelypteris torresiana under the combinational administration with a AKT inhibitor

Yi Ouyang
Wuhan Institute of Technology
Lin Wang
Wuhan Institute of Technology
Xincai Hao
xincaih@yeah.net

Hubei University of Medicine https://orcid.org/0009-0006-5766-5195

Research Article

Keywords: Interaction, Flavonoid, Macrothelypteris torresiana, AKT phosphorylation

Posted Date: April 22nd, 2024

DOI: https://doi.org/10.21203/rs.3.rs-4140875/v1

Abstract

The combinational application of herbal extract with chemical synthetic medicines is a very common therapeutic scheme for various disease. People have explored lots of combinations of natural medicine and chemical synthetic medicines to increase efficacy and reduce side effects in long lasting clinical medication. Our work found that the extract of *Macrothelypteris torresiana* could interfere with the inhibition of AKT phosphorylation induced by wortmannin in a concentration dependent manner, and the interaction mechanisms were elucidated by concentration-effect analysis and pharmacological evaluation. The study found the interaction is mainly attributed to the competitive inhibition between two flavonoids in the extract of *Macrothelypteris torresiana* and wortmannin, which competitively bind with the P110 subunit in PI3K complex. The study also found that, due to the hyperphosphorylation in the breast tumor cells, the pharmacological benefits based on the interaction are correlated with the concentration of *Macrothelypteris torresiana* extract in the combinational administration schemes. The combinational administration with 10 μg/mL EM and 0.5 μM wortmannin, a classic inhibitor of AKT, could down-regulate the AKT phosphorylation level in the tumor cells, meanwhile protecting the normal cells. The finding supports the idea of side effect reduction by combinational administration of low concentration of natural medicine and chemical synthetic medicine.

Introduction

Herbal extracts have been used in treatments of human diseases since the dawn of medicine and continuing until now (Newman et al. 2003). *Macrothelypteris torresiana*, a fern with wide distribution in southeast China (Mondal et al. 2017), is used in the prevention and treatment of many pathological conditions. The effects could be attribute to the abundance of flavonoid compounds, which could participate in various redox reactions due to their phenolic characteristics (Martens et al. 2005). In addition to the antioxidant activities, studies further proved the potent pharmacological activities in some of the flavonoids due to their special B-ring structure (Chang HL et al. 2008).

Flavonoids are considered in general as beneficial and healthy metabolites, and were even suggested to be vitamin P (Egert et al. 2011). People could benefit from the biochemical process regulation on various levels triggered by flavonoids in daily diet (Dias et al. 2012). Thus, to understand the efficacy of herbal extracts, studies always start with the isolating of active flavonoids (Chemat et al. 2012), and then explain the efficacy of extract combined with qualitative and quantitative analyses on the active flavonoids (Brusotti et al. 2014)0. In clinical medication of China, people prefer to take herbal medicines and chemical synthetic medicines simultaneously in order to recover from illness rapidly and reduce side effects (Butler et al. 2014). However, the interactions between flavonoids and chemical synthetic medicines still could occur during medication (Williamson 2001), and further interfere with the efficacy of flavonoids or chemical synthetic medicines (Heinemann et al. 2012), the interactions may lead to many uncertain pharmacodynamic appearances. The major reasons for the interactions could be boiled down to the competitive binding behavior of the compounds on the same targets (Wagner et al. 2009),

which affect the original structure-activity relationships, and then generate the interactions observed at pharmacological or pathological level (Koehn et al. 2005).

The serine/threonine kinase AKT is a critical signaling node protein that regulates a myriad of cellular functions, and the AKT activation levels in tumor and normal cell lines vary a lot (Harrison et al. 2014), which are providing the theoretical basis for the development of anti-tumor medicines (Sonnenburg et al. 2001). The AKT signaling cascade is initiated by the activation of phosphoinositide 3-kinase (PI3K), and completely activated by the phosphorylation on both Thr308 and Ser473 residues (Martini et al. 2014). Thus, the PI3K subunits, p110 and p85, attract the attention for the development of AKT inhibitors (Janku et al. 2018). However, considering the extensive cascading effects in AKT pathway, the control of side effects of AKT inhibitors has always been a research hotspot. Phytomedicine studies in our group indicated the flavonoids in *M. torresiana* could down-regulate the AKT phosphorylation levels in breast tumor cells (Liu et al. 2019). Meanwhile, studies found that the flavonoids can also meliorate the AKT dysregulation in normal cells (Prasad et al. 2010). Wortmannin is a potent and classic inhibitor for P110 subunit in PI3Ks complex (Powis et al. 1994). Our study aims to determine the concentration-effect relationship and the interaction mechanism that can achieve therapeutic advantages between the extract of *M. torresiana* and wortmannin. The broader significance of this work lies in that the regulation of AKT phosphorylation level in normal cells mediated by flavonoids can reduce side effects in the combinational treatment with AKT selected inhibitors.

Materials and Methods

Extract Preparation

The *M. torresiana* was collected around Kuzhulong village sited in the Enshi Tujia and Miao autonomous prefecture, Hubei province, China. The specimen was checked against Flora Republicae Popularis Sinicae and kept in School of Chemical Engineering & Pharmacy, Wuhan Institute of Technology. The rhizome of *M. torresiana* was dried and ground to powders (30 mesh). The powders were soaked and extracted with EtOH: H_2O (7:3 v/v) 3 times with reflux, the pH of reflux solution was titrated with 0.1M HCl to 5. After filtration, the reflux solution was further eluted by polyamide column to enrich flavonoids, the ethanolic extract of *M. torresiana* (EM) was collected and evaporated (< 50°C) to obtain the crude extract. The crude extract was suspended in water to remove water-soluble impurities. The precipitate was collected and stored at 4°C until use.

Potential therapeutic targets analysis

The targets of the flavonoids were collected from database and our previous studies (Singh DB et al. 2022). The protein-protein relation and protein-target relation were collected from STRING (Jensen et al. 2009). The above relations were integrated to constitute the compound-target (C-T) network and target-disease (T-D) network using Cytoscape 3.6.1 software (Shannon et al. 2003). The network topological properties were performed by Network Analyzer module of Cytoscape (Killcoyne et al. 2009). The degrees of nodes were defined as the number of edges connecting with them, representing the

importance of nodes in a network. Nodes were scaled to the different degree and colored by group. The association among phylum was ranked by closeness centrality, betweenness centrality, degree, and average relative abundance of each phylum. The biological process and molecular function bioinformatics between the targets and flavonoids were analyzed by gene ontology (GO) (Bindea et al. 2013) and Kyoto Encyclopedia of Genes and Genomes (KEGG) (Bindea et al. 2009) by GlueGo module.

The content determination and structure identification

The contents and structures of the flavonoids in EM were detected by Thermo LC-MS/MS system (Fisher scientific, CA, USA). LC separation was carried out on LC equipped with Hypersil C18 chromatographic column. The mobile phase was delivered at a flow rate of 0.20 mL/min by a binary gradient elution system consisting of 0.1% formic acid in water (A) and acetonitrile (B) using a gradient program as follows: 0–10 mins, 5–30% A;10–20 mins, 30–65% A; 20–50 mins, 65% A. The column temperature was set at 30°C. The detection wavelength was set at 254 nm. The eluent separated by LC was pumped directly into the Orbitrap mass spectrometer (Thermo LTQ-XL), parameters were set as follows: negative ion electrospray, auxiliary gas (N_2) pressure 40 psi, auxiliary gas (He) flow rate 9 L/min, applied probe voltage 4000 V and collision energy 45% of 5 V for MS/MS. Mass spectrometry was conducted in full scan and automatic multiple stage fragmentation scan modes over an m/z range of 100 ~ 800. The operating parameters were optimized for each analyte, and the data recorded were processed by Thermo Xcalibur.

Cells culture and anti-proliferation assay

Human breast epithelial tumor (MCF-7) and mammary fibroblasts (Hs578bst) cell lines were obtained from Tongji Hospital, Wuhan, China, and cultured in RPMI 1640 or DMEM medium supplemented with 10% FBS and 100 U/mL penicillin-streptomycin in an atmosphere of 5% CO_2 at 37°C in a humidified incubator. Wortmannin and MTT were purchased from *J&K* Scientific. Apigenin, naringenin, quercetin and kaempferol were purchased *Aladdin* Reagent. Protoapigenone, 5,7-dihydroxy-2-(1-hydroxy-2,6-dimethoxy-4-oxo-cyclohex)-chromen-4-one, 2-(1,4-dihydroxy-cyclohexyl)-5,7-dihydroxy-chromone and DEDC were kindly donated form professor Ruan and were identified by HPLC with purity more than 98%. The viability rates of MCF-7 and Hs578bst cells were determined by MTT assay. Cells were seeded in a 96-well plate by adding growth medium to reach different administration concentrations. In addition to be a positive control, 0.5 μM Wortmannin involved itself in the combinational administration with EM and flavonoids. The viability rates were represented by the absorbance at 540 nm read by microplate reader (Power-Wave XS, Bio-Tek) and converted to percentage rates to the vehicle control (0.1% DMSO).

Annexin V/PI apoptosis assay

Apoptotic cells were identified by Annexin V/ propidium iodide (PI) apoptosis detection kits (Multi-Sciences Biotech, Hangzhou). MCF-7 and Hs578bst cells were seeded in 6-well plates and exposed to the agents for 24 h. After harvested and washed with cold phosphate buffered saline (PBS), the collected cells were resuspended in binding buffer, and then were incubated for 5 mins in dark after adding annexin V and PI. Finally, the stained cells were analyzed by flow cytometry (Beckman FC500, USA).

Cell morphological assay

The MCF-7 and Hs578bst cells were seeded in 24-well plates and treated with indicated concentrations of agents for 24 h, and then stained with 10 μg/ml of Hoechst 33258 for 10 min at 37°C. After washed with cold PBS, the stained cells were imaged using fluorescence microscope (Nikon TE2000-S, Japan).

Western Blot assay

The MCF-7 and Hs578bst cells were co-cultured with EM and Wortmannin in different concentrations labeled on the top of Fig. 5a and c. After the protein content determination, the samples were separated by 12% SDS-PAGE and electro-transferred to polyvinyldifluoride membranes. The membranes were blocked with 5% (w/v) non-fat dry milk for 2 h and incubated with primary antibodies AKT1, p-AKT1^{Thr308} and p-AKT1^{Ser473} (Santa Cruz, CA) overnight at 4–8°C. The blots were washed three times in a TBST buffer, followed by an incubation for 1 h at room temperature with the horseradish peroxidase-conjugated specific secondary antibodies. Then, the blots were visualized by using an enhanced chemiluminescence detection system. The bands densitometric was determined by gel documentation system (ShineTech, GelAnalyse). The data was normalized using β-actine as internal control, with the vehicle control (0.1% DMSO) as 100%.

Enzyme-linked immunosorbent assay (ELISA)

Sandwich ELISA was applied to detect the amount of AKT1, p-AKT1^{Thr308} p-AKT1^{Ser473}, P85 and P110. The procedure refers to the instruction of ELISA kits (JinYibo life-tech, Nanjing, China). The ELISA plates were pre-coated with capture antibodies in PBS for 12 h. After co-cultured with 0.5 μM wortmannin and 0.5 μM COM 1–8 in combination and alone, the samples were added to wells and incubated for 1 h with 200 μL/well of 1% BSA in PBS, subsequently, the wells were washed with PBS. And then the plates were incubated for 2 h with biotinylated detection antibodies to bound the analyte adsorbed on the wells, the plates were washed and further incubated with HRP-conjugated avidin for 45 mins. Finally, the plates were developed by adding 50 μL of tetramethylbenzidine. The protein amount values were calculated by plotting absorbance at 450 nm with a plate reader (PowerWave XS, Bio-Tek).

Computational Study

The structure model of P110 subunit (3R7Q) retrieved from Protein Data Bank were further fitted and predicted by SYBYL-X 2.0 software. The compound structures were prepared by a molecule minimization computational module, meanwhile the protein was processed by assigning bonds, adding hydrogens and fixing residues. The protein pockets were analyzed and constructed, and then the ligand mode was employed to dock the compounds and protein. At last, the files were merged and exported to PYMol software to generate the docking graphs.

The interaction verification of EM and wortmannin

The EM with smaller concentration gradient difference and 0.5 μM wortmannin were co-cultured with the MCF-7 and Hs578bst cells to verify the interaction of EM and wortmannin. Meanwhile, the concentration

of COM3 and COM8 in the different concentration of EM were convert to μM and applied to the combinational treatment with 0.5 μM wortmannin. The expression levels of AKT1, p-AKT1^{Thr308} and p-AKT1^{Ser473} were determined by ELISA described in above.

Statistics

All data were done at least three times. Data were analyzed using SPSS 20.0 software (SPSS, USA). Results were presented as mean ± standard deviation (SD) and evaluated by one-way ANOVA followed by the Dunnett post hoc test used for multiple comparisons.

Results and discussion

The compound identification

As shown in Fig. 1a and b, the quasi-molecular ion $[M-H]^-$ peaks of the eight compounds, abbreviated as COM 1–8 in the paper, are in coincided with the molecular weight minus one. Besides the quasi-molecular ions $[M-H]^-$, the fragment ions $[M-CO-H]^-$ and $[M-CO_2-H]^-$ are also observed in the spectrums of eight flavonoids. The losses of CO and CO_2 are attributed to the contraction of the C ring (Fabre et al. 2001), a typical fragmentation pattern of flavonoids in negative ion mode.

More specifically, the compounds fall into three categories: flavone (COM 1. 3. 5. 6 and 8), flavonol (COM 4) and flavanone (COM 2 and 7) in this study. Besides the major fragments $[M-H-CO]^-$ and $[M-H-CO_2]^-$ caused by the contraction of the C ring, low abundance Retro-Diels-Alder (RDA) fragments from the flavonoids are also observed. As shown in Fig. 1d, for flavone and flavanone, a significant RDA crushing pattern in MS analysis RDA preferentially cracked from the 1, 3 position of the C-ring to generate two characteristic fragment ions $^{1,3}A^-$ and $^{1,3}B^-$. Meanwhile some fragment ions from $^{1,3}A^-$ show the A/C ring in the flavone and flavanone may further undergo the loss of CO in RDA crushing pattern. For flavonol, bearing a -OH on the C ring, a type of typical cleavage for the C ring to generate $^{1,2}A^-$ and $^{1,2}B^-$ fragment ions without loss of CO are observed.

All in all, by comparing the MS data and the retention time of each component with database of isolated chemical constituents from *M. torresiana* and *Cyclosorus* family. As shown in Fig. 1c, the compound 1–8 were identified as apigenin, naringenin, protoapigenone (Huang et al. 2010), 5,7-dihydroxy-2-(1-hydroxy-2,6-dimethoxy-4-oxo-cyclohex)-chromen-4-one (Tang et al. 2010) quercetin, kaempferol, 2-(1,4-dihydroxy-cyclohexyl)-5,7-dihydroxy-chromone (Fang et al. 2011) and (Liu et al. 2012).

The construction and analysis of C-T and T-D Network

As shown in Fig. 2b. the studies show the gene terms affected by the flavonoids are around apoptosis related pathways. Meanwhile, as shown in Fig. 2c, certain compounds point to AKT1, P110 and P85, which suggests that EM containing the above compounds could regulate AKT pathway by acting on the

above proteins. The T-D network derived from the C-T network further illustrate the target pathways and diseases of EM. Figure 2d depicts the potential biological processes, signaling pathways and targets for EM. Autophagy and apoptosis were predicted by GLUEGO module as the main biological process mediated by the eight compounds. VEGF, HIF-1 and erbB are predicted as the main pathways by which the compounds regulate autophagy and apoptosis. KEGG analysis further demonstrates that the AKT regulation and the AKT downstream cascade effects mediated by the eight compounds are the up-stream acting elements for the regulation on VEGF, HIF-1 and ErbB targets. The intricate T-D network for AKT work in two different ways. On the one hand, these compounds could regulate the AKT phosphorylation directly, on the other, these compounds could act on other signaling pathways, which are mediated by feedback regulation to stabilize the AKT phosphorylation (Hinz et al. 2019). In view of the low relevance between the compounds and downstream targets of AKT, such as VEGF, HIF-1 and Bax. The topology analyses indicated the targets of EM for AKT target exist in PI3K-AKT core pathway axis. Based on the C-T and T-D relation, breast cancer, melanoma and glioma were predicted as the target diseases of the eight compounds. Since the size of nodes represents the correlation significance in the T-D network, the T-D network reveals the similar effects in EM for these diseases. The similar efficacy could be attribute to the functional interactions within biological network, such interactions are relevant when molecular act at multiple targets in the network or when homeostatic feedback mechanisms are operative (Van Hasselt et al. 2019). Considering pharmacological experimental evidences of the eight compounds and breast cancer based on single transduction pathways, the breast cancer cells MCF-7 and normal breast cell Hs578bst were applied in this study to evaluate the systematic pharmacology properties of EM using the eight compounds as indicators.

The cell viability and apoptosis analysis

The results of cell morphology and apoptosis assays reveal the combinational administration of EM and wortmannin didn’t generated additive effects on pro-apoptosis in both the two cells. As shown in Fig. 2a, the viabilities of the MCF-7 and Hs578bst cells decrease in varying degrees in single component administration groups. The viability rates of MCF-7 and Hs578bst cells are highest in the 10 μg/mL EM treatment group and are lowest in the 0.5 uM wortmannin treatment group. With the EM concentration increasing, the viabilities of MCF-7 and Hs578bst cells decreased slightly. Besides the single component administration, the results from the combinational administration clearly show antagonism, instead of synergy, occurred between EM and wortmannin in both MCF-7 and Hs578bst cells. With wortmannin concentration fixed at 0.5 μM, the viabilities of MCF-7 and Hs578bst cells increase significantly in the 10 μg/mL EM treatment groups, subsequently, the viabilities gradually decrease as the EM concentration increase. It is worth noting that 10 μg/mL EM could trigger the interaction between the 0.5 uM wortmannin, and achieve significant viability differences between MCF-7 and Hs578bst cells. However, when the EM concentration reaches 40 μg/mL, the difference in viability rates between the two cells is not significant.

As shown in Fig. 3, the MCF-7 and Hs578bst cells co-cultured with different agents were stained by Hoechst 33258. In the control group, the MCF-7 and Hs578bst cells are generally spherical, and the DNA

is evenly distributed in the cytoplasm and nucleus. With the increase in EM concentration, the fluorescent signal inside the cells began to become less clear, which is caused by chromatin condensation and genomic DNA fragmentation. While, the chromatin of MCF-7 and Hs578bst in 0.5 μM wortmannin administration groups undergo a phase change from a heterogeneous, genetically active network to an inert, highly condensed form, and finally lead to a structural breakage in nuclei and membrane. Interestingly, the cells appear to be more normal physiological states in the combinational administration groups. The cells became intact, abundant in organelle and with integral nucleus DNA. The results of apoptotic morphology show the interaction between EM and wortmannin.

In the Annexin-V /PI apoptosis assay, stained cells simultaneously with Annexin-V and propidium iodide allows the discrimination of intact cells (quadrant LL), early apoptotic cells (quadrant LR), and necrotic cells (quadrant UR). As shown in Fig. 4a-h, the apoptosis rates of MCF-7 cells are the highest in 0.5 uM wortmannin treatment groups, and the apoptosis rate increase over the growth of EM concentration in EM single treatment group. When the cells were treated simultaneously with EM and wortmannin, the apoptosis rates of MCF-7 cells decrease with the growth of EM concentration in a concentration-dependent manner. As shown in Fig. 4a$-h$, the apoptosis rates of the Hs578bst cells are also the highest in 0.5 uM single wortmannin treatment group. Figure 4a$-d$ shows that the apoptotic rates increase slightly with the growth of EM concentration. As can be seen from Fig. 4e$-h$, with wortmannin at 0.5 uM, the apoptotic rates keep at a relatively low level in the combinational treatment groups.

It is noteworthy that the apoptosis rate gap between the Hs578bst and MCF-7 cells is obvious under the treatment of 10 μg/mL EM and 0.5 μM wortmannin, while the inter group apoptosis rate gap became less obvious under the treatment of 40 μg/mL EM and 0.5 μM wortmannin. The comparison of Fig. 4e-h and Fig. 4e$-h$ illustrate a more sensitive effecy of EM against 0.5 μM wortmannin existed in the Hs578bst cells than that in the MCF-7 cells. The lower apoptosis rate caused by low-dose agents is conducive to protection of normal cells, while the higher apoptosis rate caused by high-dose agents is conducive to elimination of malignant cells. The linear dose effect relation properties of EM and wortmannin hinder the single component administration to achieve the above two points at the same time. However, the interaction between EM and wortmannin makes it possible to achieve the above two points at the same time.

The AKT phosphorylation level determination

The study further focused on the AKT phosphorylation in the two cells. As shown in Fig. 5, the steady AKT1 expression levels under all administration show that the EM and wortmannin could hardly affect the transcription of AKT1 in the two cells. Figure 5a and b show that the expression levels of p-AKT1^{Thr308}and p-AKT1^{Ser473} were slightly down-regulated by EM in a concentration-depending manner in the MCF-7 cells. As a potent AKT phosphorylation inhibitor, the p-AKT levels in the 0.5 μM wortmannin treatment group is the lowest among all groups. Besides the single component administration groups, the lane 5–7 in Fig. 5a supports the conclusion of the interaction between EM and wortmannin. Although EM and wortmannin could both inhibit AKT phosphorylation in varying degrees, the phosphorylation inhibition of wortmannin is antagonized by EM in the combinational treatment groups. The lane 5–7 of

Fig. 5a show the AKT phosphorylation inhibition induced by wortmannin are more likely to be antagonized by high concentration of EM in the MCF-7 cells.

Antagonism was also observed in the Hs578bst cells. As show in Fig. 5c and d, with the increase in EM concentration, the expression levels of p-AKT1^{Thr308}and p-AKT1^{Ser473} in EM group decrease slightly. The expression levels of p-AKT1^{Thr308}and p-AKT1^{Ser473} bottomed out at 0.5 μM wortaminn treatment group. Similarly, the combinational treatment scheme promotes the antagonism instead of synergy occurred between EM and wortmannin in the Hs578bst cells. By comparing the AKT phosphorylation levels in the two cells under the same combinational administration, it can be found that the interaction in the normal cells is more sensitive than that in the tumor cells to the EM concentration. The different results between the two cells can be attribute to the hyperphosphorylation in tumor cells over that in normal cells (Comsa et al. 2015). Given an extensive correlation between AKT phosphorylation and downstream targets, the application of low concentration of EM combined with wortmannin could achieved a balance between the viability in the Hs578bst cells and the apoptosis induction in the MCF-7 cells.

The AKT-related target expression analyses

Since the flavonoids are the pharmacological active basis for EM, the results of combinational administration with COM 1–8 and wortmannin at the equal concentration of 0.5 μM further reveal the underlying reasons for the interaction between EM and wortmannin. As shown in Fig. 6i, the P110 expression levels in COM 3 and 8 administration groups are lower than that in COM 1, 2, 4, 5, 6 and 7 administration groups. Thus, the AKT phosphorylation levels in COM 3 and 8 treatment groups are lower than that in COM 1, 2, 4, 5, 6 and 7 treatment groups in the Hs578bst cells. On the contrary, when the Hs578bst cells were co-cultured with 0.5 μM wortmannin and COM 1–8, the AKT phosphorylation levels in COM 1, 2, 4, 5, 6 and 7 treatment groups are lower than that in COM 3 and 8 treatment groups.

As shown in Fig. 6m, like the Hs578bst cells, the expression levels of AKT1 and P85 fluctuate in a small range in all administration groups in the MCF-7 cells. The notable antagonism against wortmannin also occurred in the groups treated with COM 3 and 8. These results suggest that the similar antagonism between EM and wortmannin in the Hs578st cells is mainly due to COM 3 and 8, which should be attribute to the potent affinity between the COM 3, 8 and targets. The high affinity between the compounds and targets contributed to the better pharmacological activities for COM 3 and 8 when administered alone, but they can also form competitive binding behavior with wortmannin to the identical target, thus interfere with the target binding of wortmannin. The color contrast between Fig. 6m and Fig. 6i reveal a more distinct antagonism in the MCF-7 cells than that in the Hs578bst cells under the same administration schemes, which is also due to the AKT hyperphosphorylation in the MCF-7 cells.The Fig. 6a-h illustrate the affinity difference at P110 target based on the structural difference. The B ring of COM 3 and 8 form hook-like structure with the protein pocket, and the hydrogen bonds form between the carbonyl oxygen at the B ring and the amino acid residue of protein. The hook-like binding mode and the hydrogen bonding force contribute to the high affinity between COM 3 and 8 and protein pockets, thus obstruct the binding between P110 protein and wortmannin.

The concentration-dependent interaction of wortmannin and the EM

In the last part, we set the concentrations of COM3 and COM8 equal to their concentrations in EM to quantify this interaction relationship in the both the two cells. As shown in Fig. 7a and d, the AKT phosphorylation levels are more likely to reach a plateau range close to the blank control at low concentrations of EM in the Hs578bst cells than that in the MCF-7 cells. The differential levels on the interaction between EM and wortmannin in the two cells prove that the normal cells are more sensitive to the concentration of EM in combinational treatment. The Fig. 7b, c and Fig. 7e, f illustrate the contributions of COM3 and COM6 to the phosphorylation inhibition antagonism in the MCF-7 cells and in the Hs578bst cells respectively. COM3 can reverse the AKT phosphorylation inhibition induced by 0.5 μM wortmannin above the concentrations five times greater than that of wortmannin, and maintain a concentration-dependent antagonism relationship until 32.51 μM. Subsequently, the phosphorylation levels decrease in both the two cells treated with COM3 of concentration at 43.35 μM. Similarly, COM6 can attenuate the phosphorylation inhibition induced by 0.5 μM wortmannin, and due the low content of COM6 in EM, the interaction curves shown in Fig. 7c and f exhibit a more typical concentration dependent linear relationship.

Conclusion

The study established a combinational administration scheme of EM and wortmannin from the perspective of phytomedicine. The study concluded that the concentration of extract in combinational administration scheme with synthetic medicines is highly related to the outcomes of interaction. An appropriate concentration ratio can protect the normal cells by stabilizing the AKT phosphorylation level, and minimize the interference with the AKT phosphorylation inhibition induced by wortmannin in the tumor cells. The following studies will explore whether the flavonoids in *Macrothelypteris torresiana* has similar effects on the AKT phosphorylation change either caused by other AKT inhibitors or caused by the ripple effects from other signal pathways.

Abbreviations

AKT, Protein kinase B; PDK-1, 3-phosphoinositide dependent protein kinase-1; PI3K, phosphatidylinositol 3 kinase; FBS, Fetal Bovine Serum; MTT, Thiazolyl Blue Tetrazolium Bromide

Declarations

Authors' contributions: ZL: conceptualization, data curation, writing - original draft, project administration, funding acquisition. OY: methodology, data curation, formal analysis, writing original draft. WL, investigation, methodology, data curation, validation. HC, conceptualization, funding acquisition, resources, writing - review and editing, supervision.

Funding: This work was supported by the Open Project of Hubei Key Laboratory of Wudang Local Chinese Medicine Research (Hubei University of Medicine) (Grant No. WDCM2022013), and the innovation and entrepreneurship project of Hubei Province (20201049001), and the young talent grant of Wuhan Institute of Technology (237114)

Competing interests/COI statement: The authors have no competing interests to declare that are relevant to the content of this article.

References

1. Bindea G, Galon J, Mlecnik B (2013) CluePedia Cytoscape plugin: pathway insights using integrated experimental and in silico data. Bioinformatics 29:661–663. http://dx.doi.org/10.1093/bioinformatics/btt019
2. Bindea G, Mlecnik B, Hackl H, Charoentong P, Tosolini M, Kirilovsky A, Fridman WH, Pages F, Trajanoski Z, Galon J (2009) ClueGO: a Cytoscape plug-in to decipher functionally grouped gene ontology and pathway annotation networks. Bioinformatics 25:1091–1093. http://dx.doi.org/10.1093/bioinformatics/btp101
3. Brusotti G, Cesari I, Dentamaro A, Caccialanza G, Massolini G (2014) Isolation and characterization of bioactive compounds from plant resources: The role of analysis in the ethnopharmacological approach. J Pharmaceut Biomed 87:218–228. http://dx.doi.org/10.1016/j.jpba.2013.03.007
4. Butler MS, Robertson AAB, Cooper MA (2014) Natural product and natural product derived drugs in clinical trials. Nat Prod Rep 31:1612–1661. http://dx.doi.org/10.1039/c4np00064a
5. Chang HL, Su JH, Yeh YT, Lee YC, Chen HM, Wu YC, Yuan SS (2008) Protoapigenone, a novel flavonoid, inhibits ovarian cancer cell growth in vitro and in vivo. Cancer Lett 267:85–95. http://dx.doi.org/10.1016/j.canlet.2008.03.007
6. Chemat F, Vian MA, Cravotto G (2012) Green Extraction of Natural Products: Concept and Principles. Int J Mol Sci 13:8615–8627. http://dx.doi.org/10.3390/ijms13078615
7. Comsa S, Cimpean AM, Raica M (2015) The Story of MCF-7 Breast Cancer Cell Line: 40 years of Experience in Research. Anticancer Res 35:3147–3154
8. Dias DA, Urban S, Roessner UA (2012) historical overview of natural products in drug discovery. Metabolites 2:303–336. http://dx.doi.org/10.3390/metabo2020303
9. Egert S, Rimbach G (2011) Which sources of flavonoids: complex diets or dietary supplements? Adv Nutr 2:8–14. http://dx.doi.org/10.3945/an.110.000026
10. Fabre N, Rustan I, Hoffmann E, Quetin-Leclercq J (2001) Determination of flavone, flavonol, and flavanone aglycones by negative ion liquid chromatography electrospray ion trap mass spectrometry. J Am Soc Mass Spectr 12:707–715. http://dx.doi.org/10.1016/s1044-0305(01)00226-4
11. Fang W, Ruan JL, Cai YL, Wei AH, Zhou DN, Zhang WT (2011) Flavonoids from the aerial parts of Macrothelypteris torresiana. Nat Pro Res 25:36–39. http://dx.doi.org/10.1080/14786411003766888

12. Harrison ME, Coombs MRP, Delaney LM, Hoskin DW (2014) Exposure of breast cancer cells to a subcytotoxic dose of apigenin causes growth inhibition, oxidative stress, and hypophosphorylation of Akt. Exp Mol Pathol 97:211–217. http://dx.doi.org/10.1016/j.yexmp.2014.07.006
13. Heinemann V, Haas M, Boeck S (2012) Systemic treatment of advanced pancreatic cancer. Cancer Treat Rev 38:843–853. http://dx.doi.org/10.1016/j.ctrv.2011.12.004
14. Hinz N, Juecker M (2019) Distinct functions of AKT isoforms in breast cancer: a comprehensive review. Cell Commun Signal 17:154. http://dx.doi.org/10.1186/s12964-019-0450-3
15. Huang XH, Xiong PC, Xiong CM, Cai YL, Wei AH, Wang JP, Liang XF, Ruan JL (2010) In vitro and in vivo antitumor activity of Macrothelypteris torresiana and its acute/subacute oral toxicity. Phytomedicine 17:930–934. http://dx.doi.org/10.1016/j.phymed.2010.03.006
16. Janku F, Yap TA, Meric-Bernstam F (2018) Targeting the PI3K pathway in cancer: are we making headway? Nat Rev Clin Oncol 15:273–291. http://dx.doi.org/10.1038/nrclinonc.2018.28
17. Jensen LJ, Kuhn M, Stark M, Chaffron S, Creevey C, Muller J, Doerks T, Julien P, Roth A, Simonovic M, Bork P, Von-Mering C (2009) STRING 8-a global view on proteins and their functional interactions in 630 organisms. Nucleic Acids Res 37:412–416. http://dx.doi.org/10.1093/nar/gkn760
18. Killcoyne S, Carter GW, Smith J, Boyle J (2009) Cytoscape: a community-based framework for network modeling. Methods Mol Biol 563:219–239. http://dx.doi.org/10.1007/978-1-60761-175-2-12
19. Koehn FE, Carter GT (2005) The evolving role of natural products in drug discovery. Nature reviews. Nat Rev Drug discov 4:206–220. http://dx.doi.org/10.1038/nrd1657
20. Liu HB, Jiang CY, Xiong CM, Ruan JL (2012) DEDC, a new flavonoid induces apoptosis via a ROS-dependent mechanism in human neuroblastoma SH-SYSY cells. Toxicol Vitro 26:16–23. http://dx.doi.org/10.1016/j.tiv.2011.10.002
21. Liu ZW, Cao S, Jin C, He Y, Zhou XL, Zhang H, Liu ZM (2019) The antagonism between apigenin and protoapigenone to the PDK-1 target in Macrothelypteris torresiana. Fitoterapia 134:14–22. http://dx.doi.org/10.1016/j.fitote.2019.02.005
22. Martens S, Mithöfer A (2005) Flavones and flavone synthases. Phytochemistry 66:2399–2407. http://dx.doi.org/10.1016/j.phytochem.2006.01.004
23. Martini M, De-Santis MC, Braccini L, Gulluni F, Hirsch E (2014) PI3K/AKT signaling pathway and cancer: an updated review. Ann Med 46:372–383. http://dx.doi.org/10.3109/07853890.2014.912836
24. Mondal S, Ghosh S, Seru G, Chekuboyina SVG, Samal M (2017) Hepatoprotective activity of Macrothelypteris torresiana (Gaudich.) aerial parts against CCl4-induced hepatotoxicity in rodents and analysis of polyphenolic compounds by HPTLC. J Pharm Anal 7:181–189. http://dx.doi.org/10.1016/j.jpha.2016.12.001
25. Newman DJ, Cragg GM, Snader KM (2003) Natural products as sources of new drugs over the period 1981–2002. J Nat Prod 66:1022–1037. http://dx.doi.org/10.1021/np030096l

26. Powis G, Bonjouklian R, Berggren MM, Gallegos A, Abraham R, Ashendel C, Zalkow L, Matter WF, Dodge J, Grindey G (1994) Wortmannin, a potent and selective inhibitor of phosphatidylinositol-3-kinase. Cancer Res 54:2419–2423
27. Prasad S, Phromnoi K, Yadav V, Chaturvedi M, Aggarwal B (2010) Targeting inflammatory pathways by flavonoids for prevention and treatment of cancer. Planta Med 76:1044–1063. http://dx.doi.org/s-0030-1250111
28. Singh DB, Pathak RK, Rai D (2022) From Traditional Herbal Medicine to Rational Drug Discovery: Strategies, Challenges, and Future Perspectives. Rev Bras Farmacogn 32:147–159. https://doi.org/10.1007/s43450-022-00235-z
29. Shannon P, Markiel A, Ozier O, Baliga NS, Wang JT, Ramage D, Amin N, Schwikowski B, Ideker T (2003) Cytoscape: a software environment for integrated models of biomolecular interaction networks. Genome Res 13:2498–2504. http://dx.doi.org/10.1101/gr.1239303
30. Sonnenburg ED, Gao T, Newton AC (2001) The phosphoinositide-dependent kinase, PDK-1, phosphorylates conventional protein kinase C isozymes by a mechanism that is independent of phosphoinositide 3-kinase. J Biol Chem 276:45289–45297. http://dx.doi.org/10.1074/jbc.M107416200
31. Tang Y, Xiong CM, Zhou DN, Wei AH, Fu W, Cai YL, Ruan JL (2010) A new flavonoid from Macrothelypteris torresiana. Chem Nat Comp 46:209–211. http://dx.doi.org/10.1007/s10600-010-9570-0
32. Van Hasselt JGC, Iyengar R (2019) Systems Pharmacology: Defining the Interactions of Drug Combinations. Annu Rev Pharmacol Toxicol 59:21–40. https://doi.org/10.1146/annurev-pharmtox-010818-021511
33. Wagner H, Ulrich-Merzenich G (2009) Synergy research: approaching a new generation of phytopharmaceuticals. Phytomedicine 16:97–110. http://dx.doi.org/10.1016/j.phymed.2008.12.018
34. Williamson EM (2001) Synergy and other interactions in phytomedicines. Phytomedicine 8:401–409. http://dx.doi.org/10.1078/0944-7113-00060

Figures

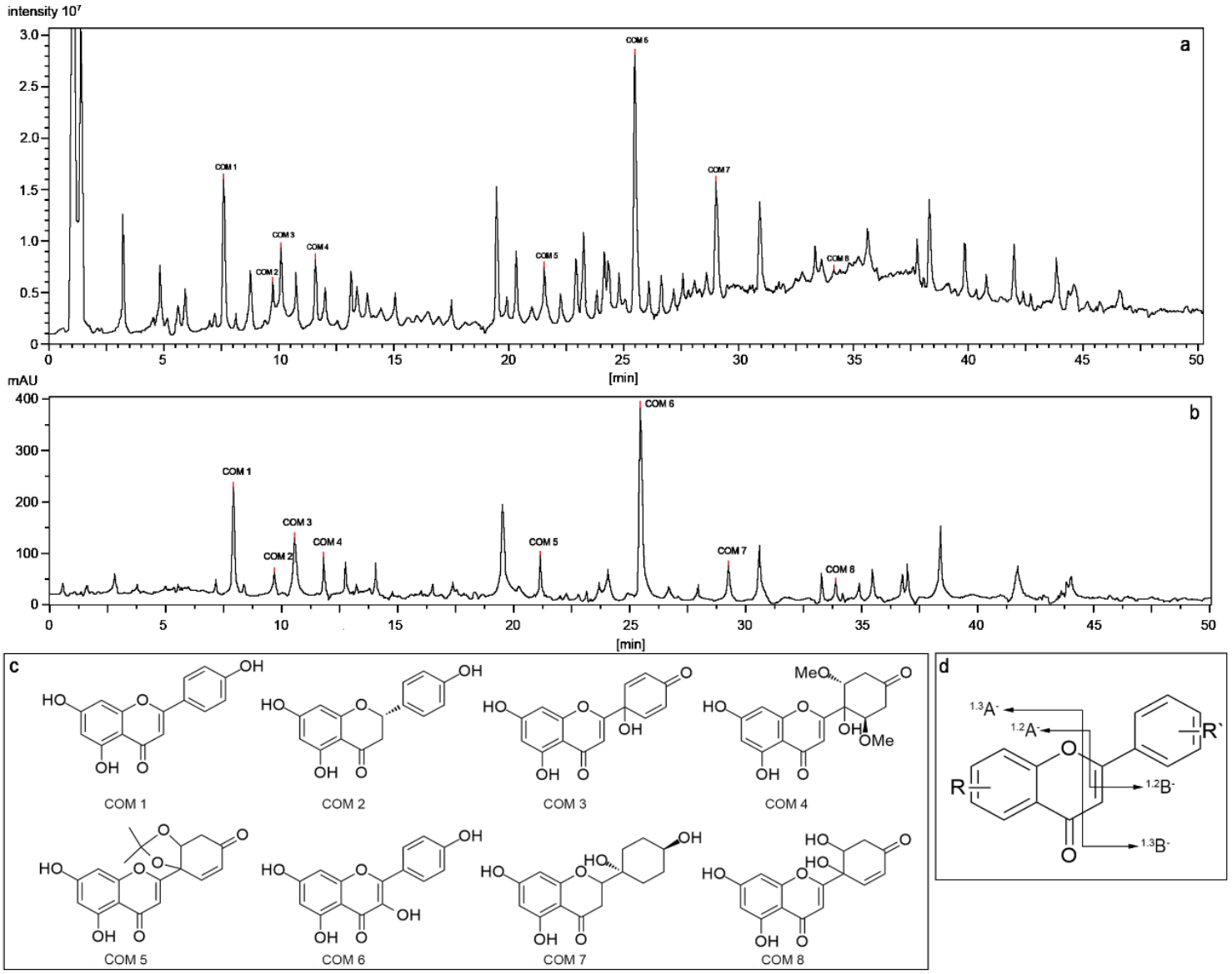

Figure 1

Component identification. a. the total ion current chromatogram. b. the UV chromatogram c. the compound structure. d the proposed fragmentation pattern for the eight compounds.

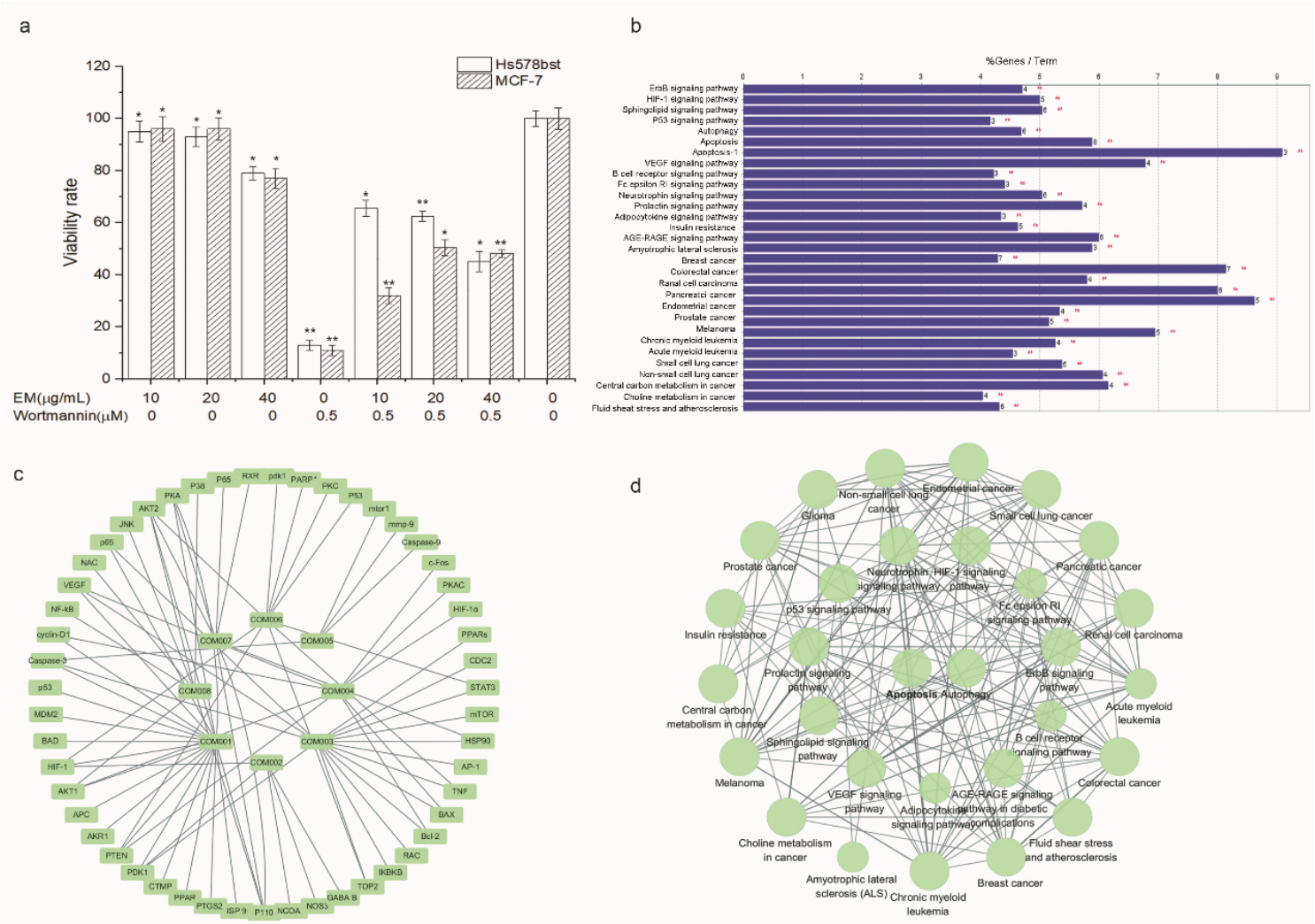

Figure 2

Systems pharmacology characteristic and viability assay of EM. a. the viability rates in the two cell lines. The data are presented as mean ± SD. *P < 0.05 and **P < 0.01 compared with 0.1% DMSO treated group. b. the GO and KEGG pathway analyses concerning the target diseases. c. the compound-target relationship. d. the GO and KEGG pathway analyses concerning the biological processes.

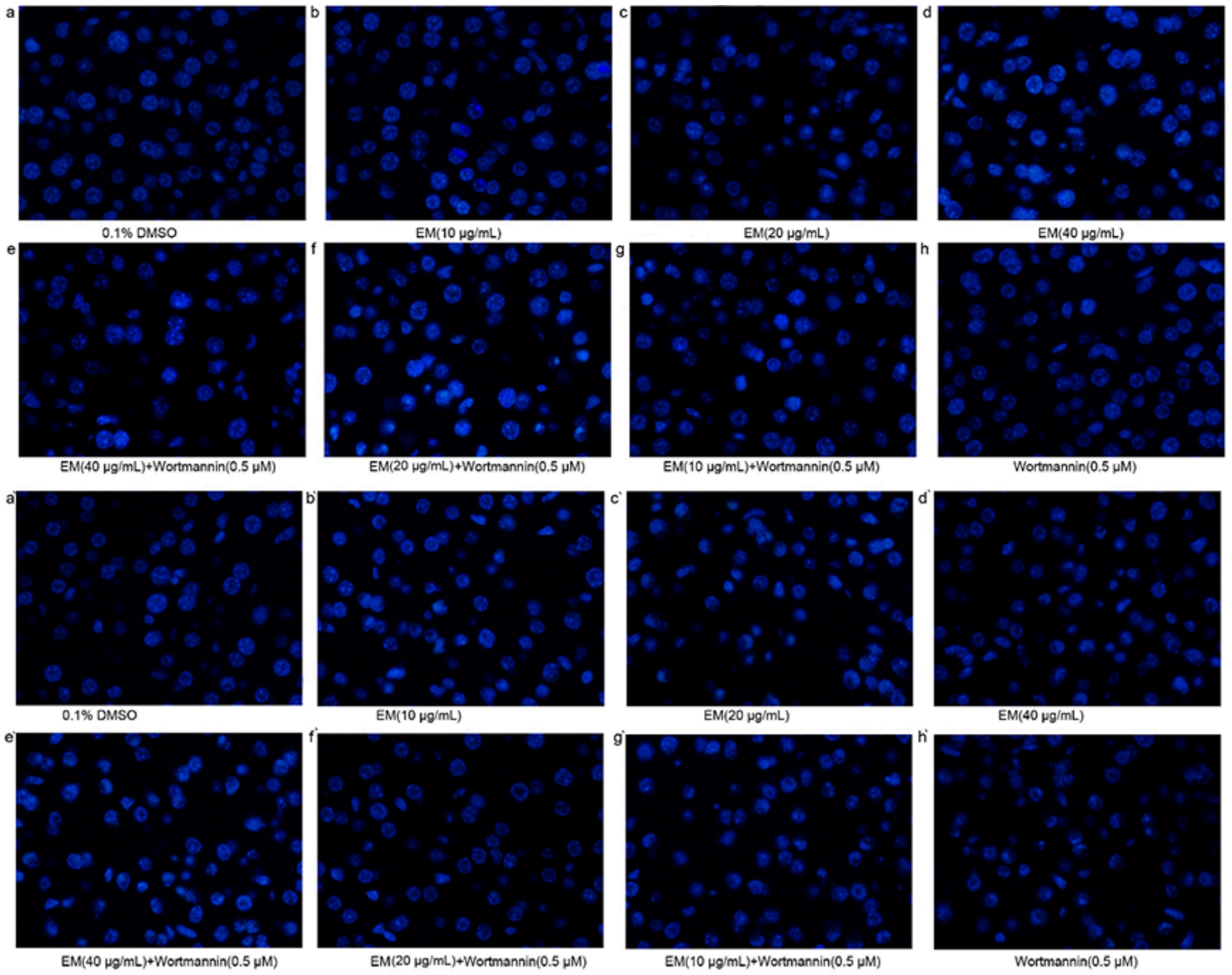

Figure 3

The apoptosis morphology of the cells treated with different administration schemes of EM and wortmannin. (a - h) in the MCF-7 cells, (a — h) in the Hs578bst cells.

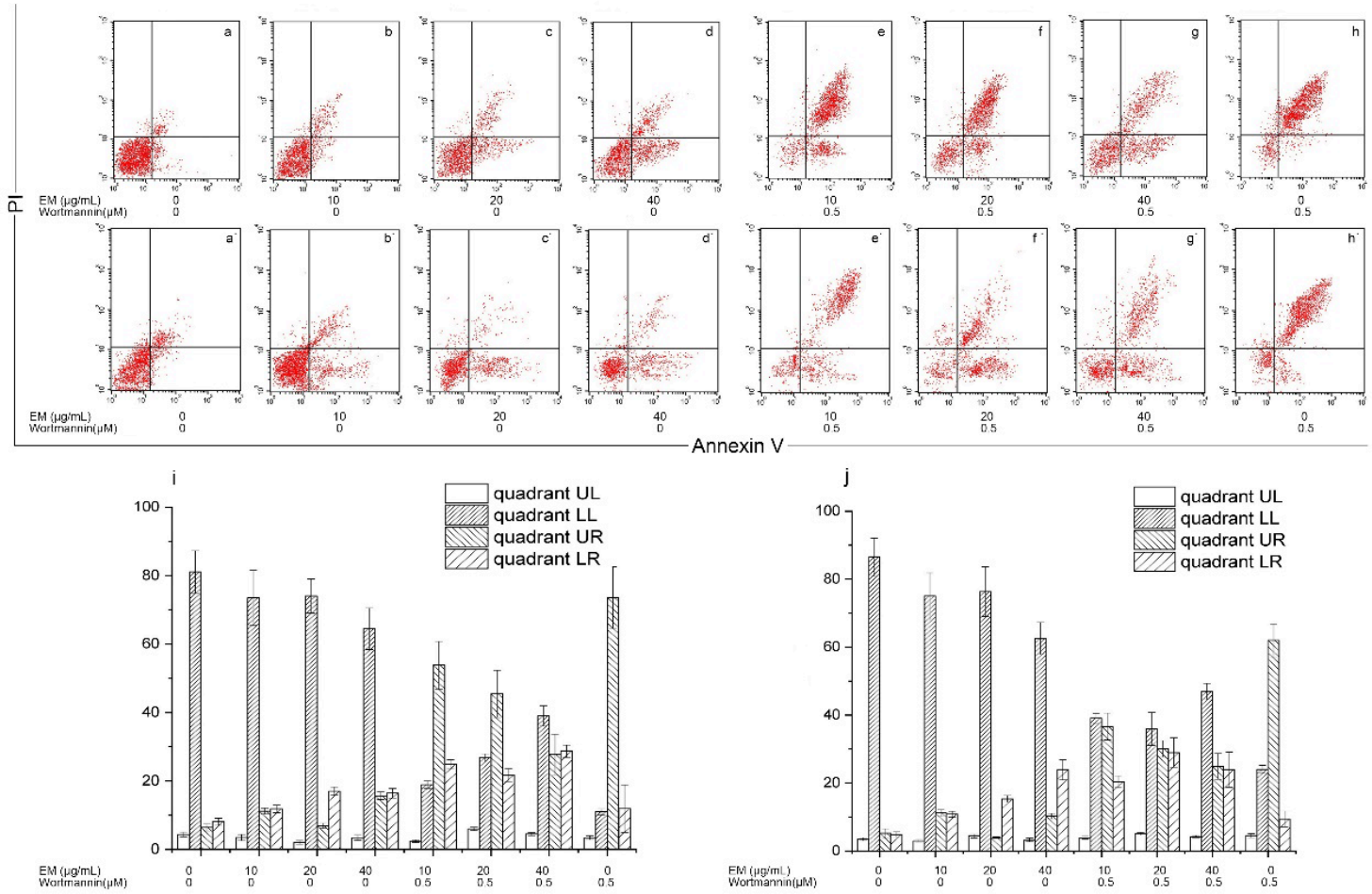

Figure 4

The cell apoptosis caused by the different administration schemes of EM and wortmannin. (a-h) in the MCF-7 cells, (a— h) in the Hs578bst cells, (i) the bar graph corresponding to a-h, (j) the bar graph corresponding to a— h. The data are presented as mean ± SD.

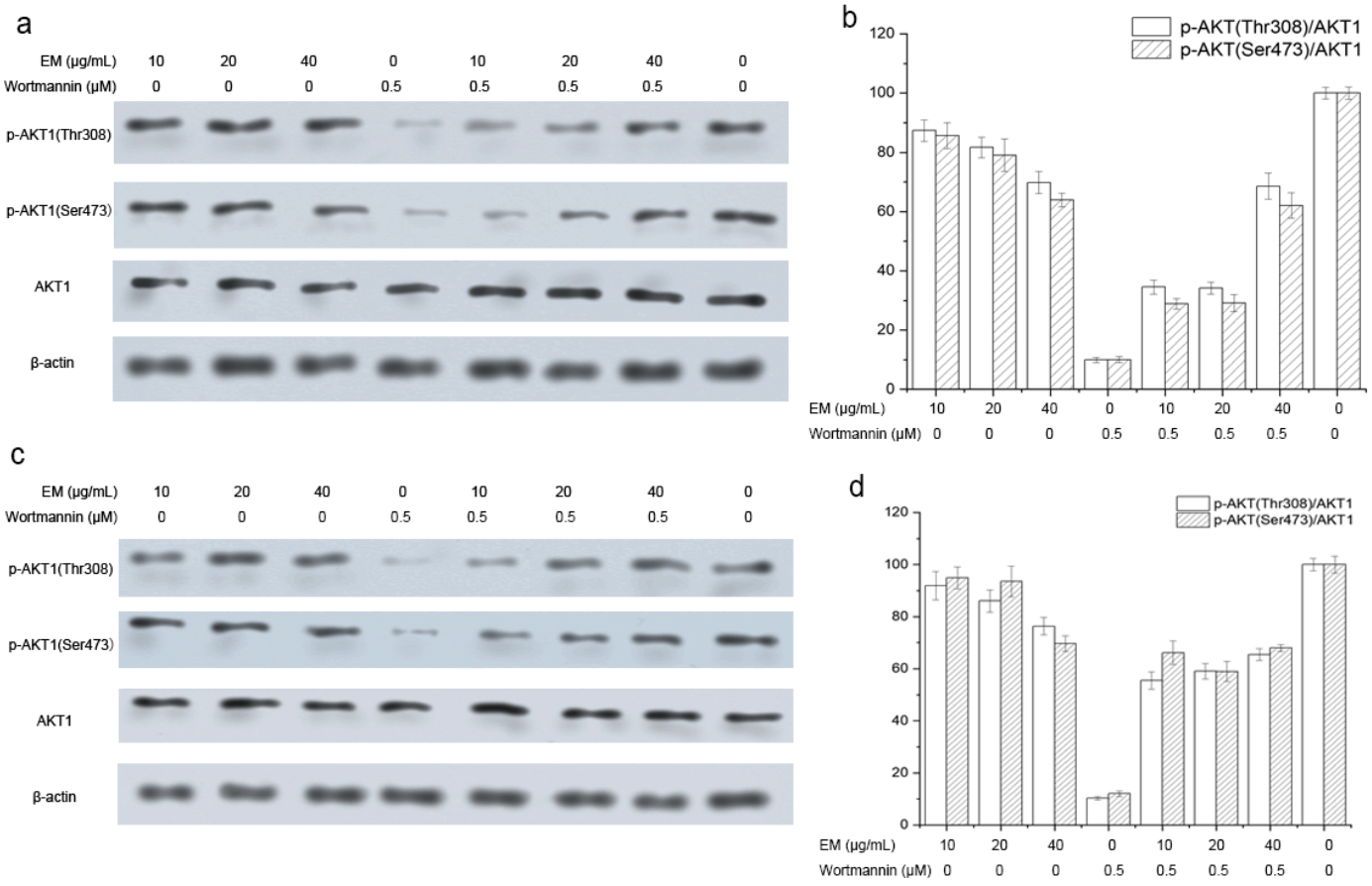

Figure 5

The AKT phosphorylation levels caused by different administration schemes of EM and wortmannin. (a) in the MCF-7 cells, (c) in the Hs578bst cells. (b) the bar graph corresponding to a, (d) the bar graph corresponding to c. The data were presented as mean ± SD. *P < 0.05 and **P < 0.01 compared with 0.1% DMSO treated group

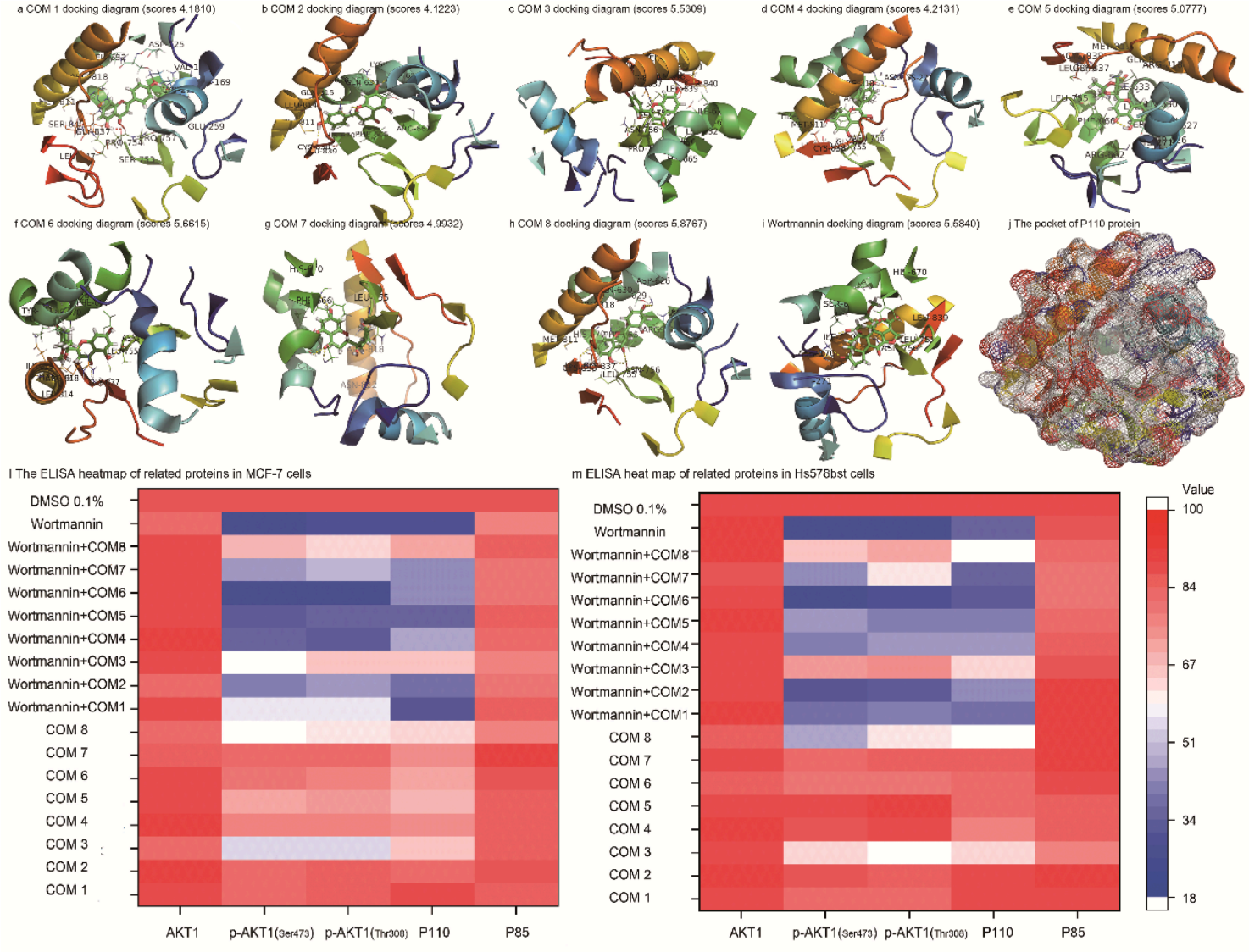

Figure 6

The docking graphs of P110 protein with different compound. (a-h) COM 1-8, (i)wortmannin, (j) the docking pocket in the P110 protein. The expression level of the AKT1, p-AKT1^{Thr308} p-AKT1^{Ser473}, P85 and P110 under different administration schemes of COM 1-8 and wortmannin determined by ELISA (l) in the MCF-7 cells and (m). in the Hs578bst cells.

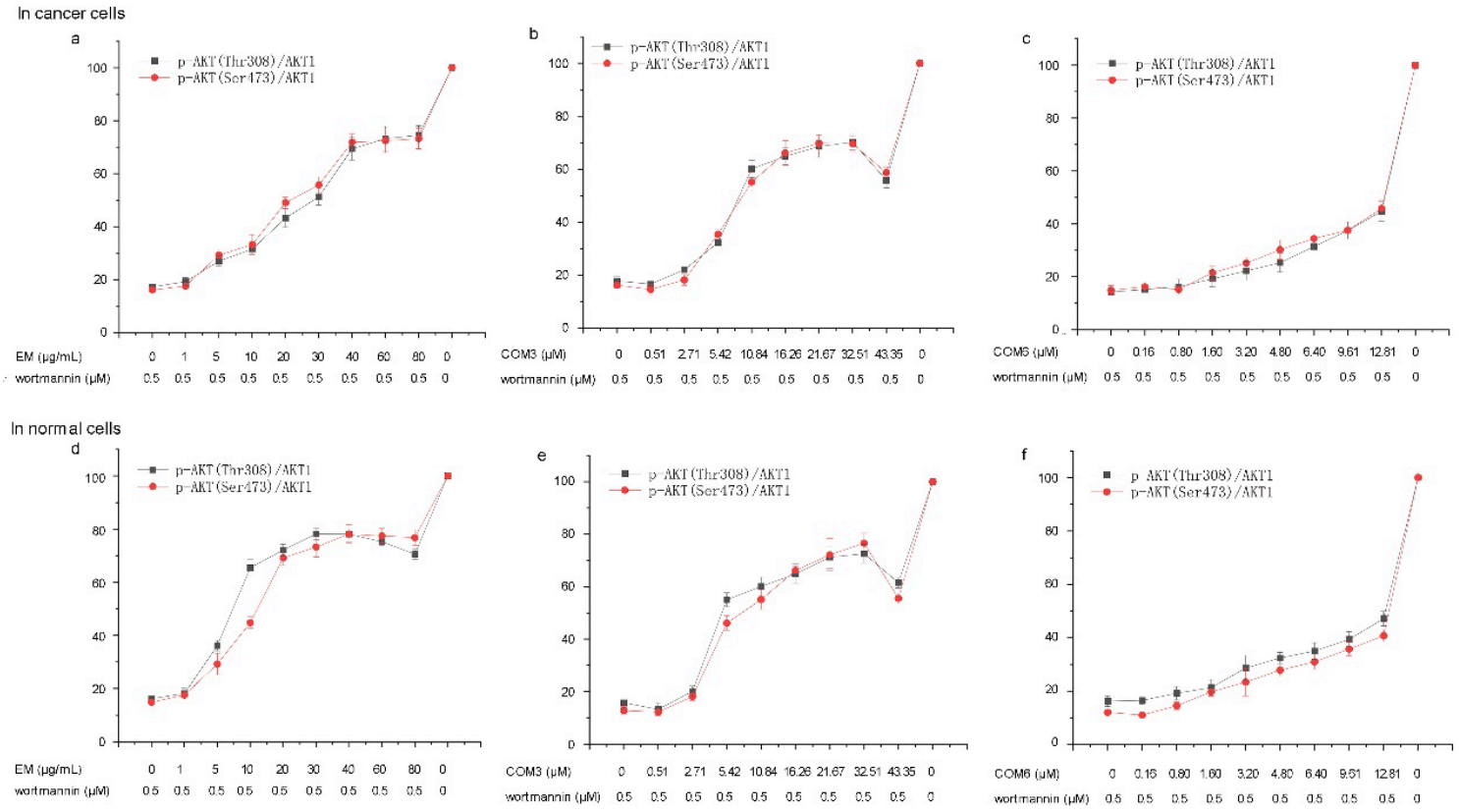

Figure 7

The concentration-depended interaction curves among the EM, COM3, COM8 and wortmannin in the MCF-7 cells (a-c) and in the Hs578bst cells (d-f). The concentrations of COM3 in Fig b and e are equivalent to the concentrations of COM3 in the EM with concentrations range from 0 to 80 μg/mL. The concentrations of COM8 in Fig c and f are equivalent to the concentrations of COM8 in the EM with concentrations range from 0 to 80 μg/mL. The data were presented as mean ± SD.

Supplementary Files

This is a list of supplementary files associated with this preprint. Click to download.

- SupplementaryMaterial.docx
- graphicabstract.png